Effect of high voltage pulse bias on stress and morphology of CA-PVD TiN Coatings

Taghavi Pourian Azar, G. & Urgen, M.

DOI 10.1080/02670844.2018.1512731
ISSN 0267-0844
ESSN 1743-2944

Publisher: Taylor and Francis

Effect of High Voltage Pulse Bias on Stress and Morphology of CA-PVD TiN Coatings

Golnaz Taghavi Pourian Azar[a] and Mustafa Ürgen[a]*

[a]*Department of Metallurgical and Materials Engineering, Istanbul Technical University, 34469, Maslak, Istanbul, Turkey*

*Corresponding author: M. Ürgen, Department of Metallurgical and Materials Engineering, Istanbul Technical University, 34469, Maslak, Istanbul, Turkey e-mail: urgen@itu.edu.tr

Effect of High Voltage Pulse Bias on Stress and Morphology of CA-PVD TiN Coatings

We investigated the role of high voltage pulse bias (HVPB) on the structural, morphological and residual stress of TiN coatings produced with Cathodic Arc Physical Vapor Deposition (CA-PVD) and compared them with the ones produced with DC bias. Annealing heat treatment was also performed for surveying stress-relieving behavior within the coatings. Preferred orientation of the coatings changed from (111) to (220) by the application of high voltage pulse bias. Coatings produced with DC bias exhibited Zone T structure, while the growth morphologies of the coatings produced with HVPB were very similar to the structures in the beginning of Zone II. Presence of Ar in the deposition environment increased the residual stress of all coatings. Intra-grain stresses of the coatings produced with DC bias were almost totally annihilated by annealing. However, for coatings produced with HVPB, stress relief magnitudes were very low indicating that intra-grain defects could not be totally annihilated.

Keywords: High voltage pulse bias; Residual stress; Morphology; TiN coating; Cathodic arc physical vapor deposition

1. Introduction

Titanium nitride (TiN) is a very well-known material that is widely applied as hard wear resistant protective coatings on cutting and forming tools [1-3]. Structure, morphology and residual stress of these coatings show a strong dependence on the deposition method and parameters. The changes induced by these variations are strongly reflected to the final properties of the coatings.

CA-PVD is widely applied for deposition of nitride-based coatings. The primary advantage of this method is its ability to produce highly ionized plasma. Ion energies of CA-PVD plasma can be further increased, or tuned by applying a negative bias applied to the substrate. Application of a DC bias during deposition leads to the formation of dense and well-adherent coatings. However, this application increases residual compressive stresses of the coatings that may be detrimental for some applications [2, 4]. On the other hand, it is well known from filtered CA systems, that using HVPB introduces an opportunity to control stress build-up of nitride-based coatings [5, 6]. Recently, we have adapted this method to unfiltered cathodic arc systems and observed similar preferred orientation changes as seen in the filtered arc systems [6, 7]. We also determined the critical role of Ar presence in the gas mixture on these changes [8].

There are many studies in the literature that explain deposition parameter-dependent preferred orientation and growth mode changes, mainly for nitride-based coatings produced with sputtering [9-12]. However, for CA-PVD coatings produced with HVPB, a systematic study that investigates the relations between bias voltage-dependent preferred orientation and growth morphology of the coatings is not present. Thus, the first aim of this study was to establish these relations for TiN coatings grown under different bias voltage modes and magnitudes with CA-PVD.

For TiN films grown with CA-PVD, the relationship between residual stress development and HVPB magnitude has already been shown in several studies [5-7, 13]. The changes in the residual stress were mainly explained by the atomic scale defect generation inside the grains and their annihilations [7, 13]. However, in these studies, the role of stress generated at the grain boundaries [14-18], which is strongly related to the microstructure of the coatings, had not been taken into account. Therefore, we also aimed to interrelate the HVPB magnitude-dependent residual stress development, with the microstructure of the coatings, by both considering atomic scale defect generation/annihilation and morphology of the coatings.

2. Experimental

A semi-industrial scale Novatech-SIE, Model: NVT-12 CA evaporation system was utilized to deposit coatings using 10 cm diameter circular Ti targets operated with a cathode current of 60 A. Metalographically polished, High Speed Steel (HSS) samples with 20 x 20 x 5 mm dimensions were used as substrates. The substrates were cleaned ultrasonically in an alkaline solution for 15 min, washed with distilled water and dried with ethanol before introducing into a vacuum chamber. Prior to initiation of the deposition, the substrates were heated, and Ti ion etched utilizing a high voltage DC bias. The deposition parameters, samples coding, and coatings thicknesses are presented in Table I. Deposition time for all the films was 15 min. During the deposition, samples were not rotated and target to substrate distance was kept constant at 15 cm.

The X-Ray Diffraction (XRD) investigations were carried out using a Philips PW3710 diffractometer equipped with a CuKα X-ray source. XRD measurements were carried out in both θ-2θ and Glancing Incidence (GI) modes. Residual stresses in the coatings were measured by X-ray tensometry technique using $\sin^2\psi$ method modified for GI X-ray diffraction. During the measurements, the incidence angle α was fixed at 2 degrees. Stresses were calculated using a-

$\sin^2\psi$ plots and symmetric biaxial stress state approach [1, 19]. For the stress evaluation, the X-ray elastic constants for the TiN stucture with (111) and (220) prefererred orientations were taken from Ref. [13], (Young's modulus, 418 GPa for (111) and 424 GPa for (220) oriented planes). Poisson ratios of (111) and (220) oriented planes were determined from Reuss's approximation [20] using elastic constants given by Perry [21]. $\mathrm{Sin}^2\psi^0$ values that correspond to the strain-free directions were estimated from '$\sin^2\psi^0=2\upsilon/1+\upsilon$' equation using the calculated Poisson ratios of (111) and (220) planes.

Surfaces of all as-deposited samples were polished and etched in sodium hydroxide + hydrogen peroxide mixture for 30 s to reveal the column boundaries and then examined by Field Emission Scanning Electron Microscope (FESEM) (Jeol 7100F). ImageJ program was used to calculate the area of grains on the etched surfaces for all as-deposited coatings [22]. Furthermore, cross-sections of the coatings were prepared and examined by Focused Ion Beam (FIB) (JEOL JEM-9320). A thin protective carbon layer was deposited on the surface before FIB milling to obtain a sharper top surface of the cross-sections. A preliminary high ion current milling (5 nA) followed by two lower ion current milling steps (0.5 nA, 0.1 nA) were used until the desired cross-sections were obtained. The obtained results for the average grain area and coatings thicknesses are also presented in Table I.

To annihilate the residual stresses, annealing heat treatment was performed on the coated samples in a vacuum furnace at 700±10 ^{o}C for 2 h, and then furnace cooled in the vacuum. The pressure at the annealing temperature was 10^{-4}-10^{-3} Pa.

3. Results and Discussion

3.1. Bias Potential-Related Texture and Morphology of the Films

TiN coatings produced with DC bias (DC-NA and DC-N) exhibited (111) preferred orientation that is typical for CA-PVD TiN coatings produced with DC bias (Fig. 1a and 2a). The cross-sectional structure was inhomogeneous along the film thickness and exhibited typical Zone T structure. It was fine crystalline at the regions adjacent to the substrate, grown as V-shaped grains in the next thickness range and became columnar in the upper part of the thick films (Fig. 3b & 4b). The presence of Ar in the deposition environment did not create any appreciable difference in the planar and cross-sectional morphology of the coatings (Fig. 3a, b & 4a, b).

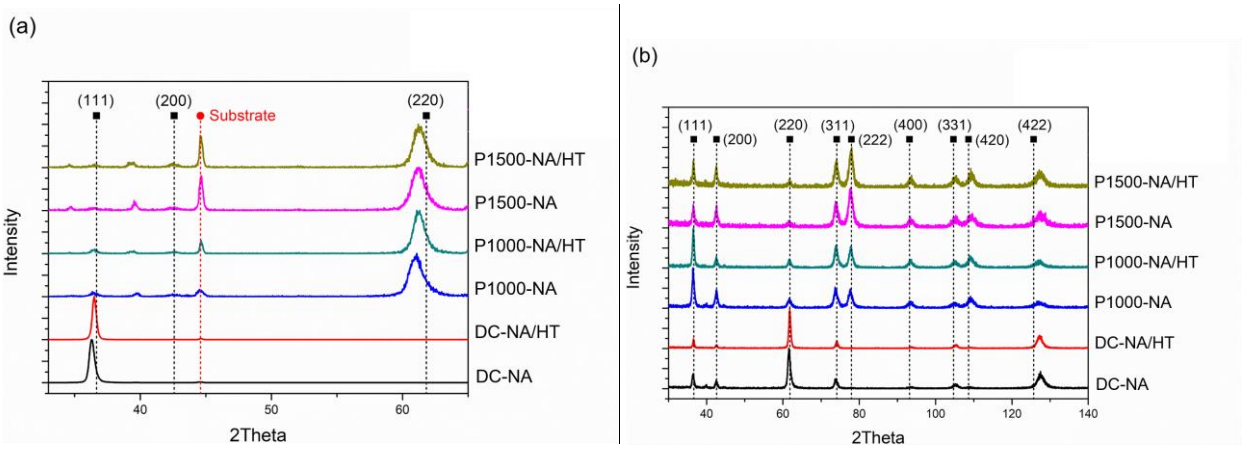

Figure 1. XRD patterns of TiN coatings deposited using different bias voltages in the N2+Ar atmosphere before and after heat treatment in (a) θ-2θ and (b) GI modes.

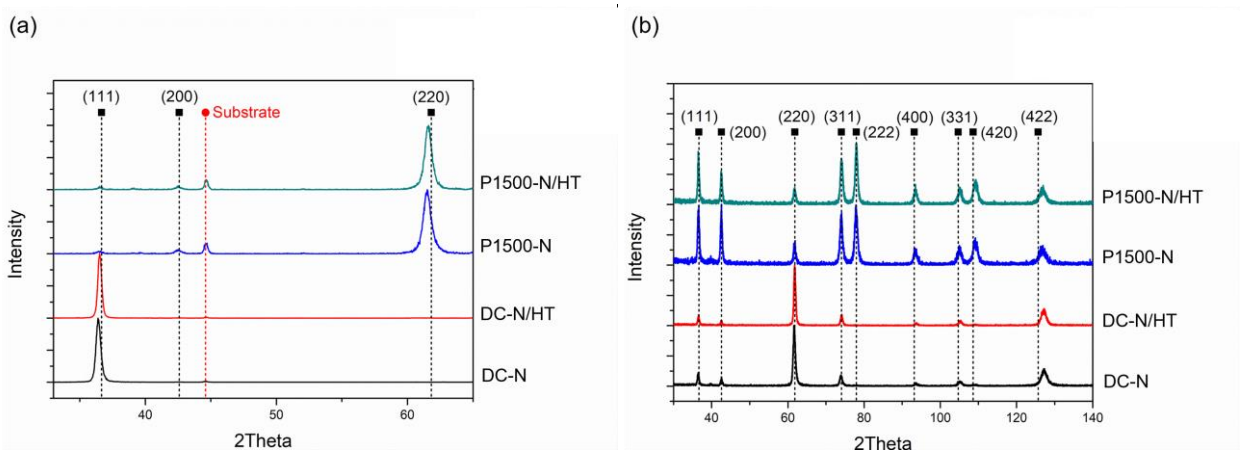

Figure 2. XRD patterns of TiN coatings deposited using different bias voltages in pure N_2 gas before and after heat treatment in (a) θ-2θ and (b) GI modes.

For TiN coatings produced using -1000 V HVPB in the mixture of N_2 and Ar, a change in the preferred orientation to (220) was observed (Fig. 1a). This type of preferred orientation is only observed when the ion energy is sufficiently high [23] and is typical for CA-PVD TiN coatings produced with HVPB [5-7, 13]. Along with the change of the preferred orientation to (220), growth mode of the coatings also changed into long and fine columns extending from the substrate and exhibitied a growth morphology that was much closer to Zone II (Fig. 3d). According to the recent zone model given by Anders [24], during the transition from Zone T to Zone II, column sizes are finer and do not show perfect columnarity. Thus, the growth morphology observed in Fig. 3d can be described as Zone II that has not acquired sufficient energy for the growth of columns.

As pulse bias voltage further increased to -1500 V, (220) orientation (Fig. 1a) and growth morphology (Fig. 3f) were preserved. But in this case, column size distribution became more homogeneous (Fig. 3e and 5). These results indicated that under the above-stated conditions, by the application of short cycles of high voltage pulses during the deposition process, the energy required for restructuring was given to the system via increasing the adatom mobility.

The most common textures for TiN films with a thickness of more than 1 μm are (111), (200) or (220), showing dependence on the deposition conditions. The textural evolution of TiN thin films is explained using thermodynamic [1, 25-28] or kinetic principles [9]. In the excellent review of Mahieu et al. [10], the relation between preferential growth and Structure Zone Model (SZM) is analyzed and evaluated for coatings produced with magnetron sputtering. According to this model, films that grow only in Zone T or Zone II exhibit preferred orientation, relying on the kinetic or thermodynamic principles, respectively. In Zone T structure, the grain boundary migration is strongly limited [29]. The overgrowth of grains with the fastest growth direction perpendicular to the substrate, leads to (111) preferred orientation in thick TiN, and a V-shaped

growth morphology was observed. On the other hand, the preferred orientation for films with Zone II structure is explained by the energy minimisation principle, since recrystallisation or restructuring can take place due to the higher mobility of atoms under this growth condition [30]. In this case, columns are oriented with the plane of the lowest surface energy ((200) orientation), or stopping energy related to channeling effect ((220 orientation). Under these conditions, an approximately straight columnar structure throughout the film thickness is observed. The combined results (preferrred orientation changes and growth morphology) of this study are in accordance with the model proposed by Mahieu et al. [10] and show its applicability to films grown with CA-PVD.

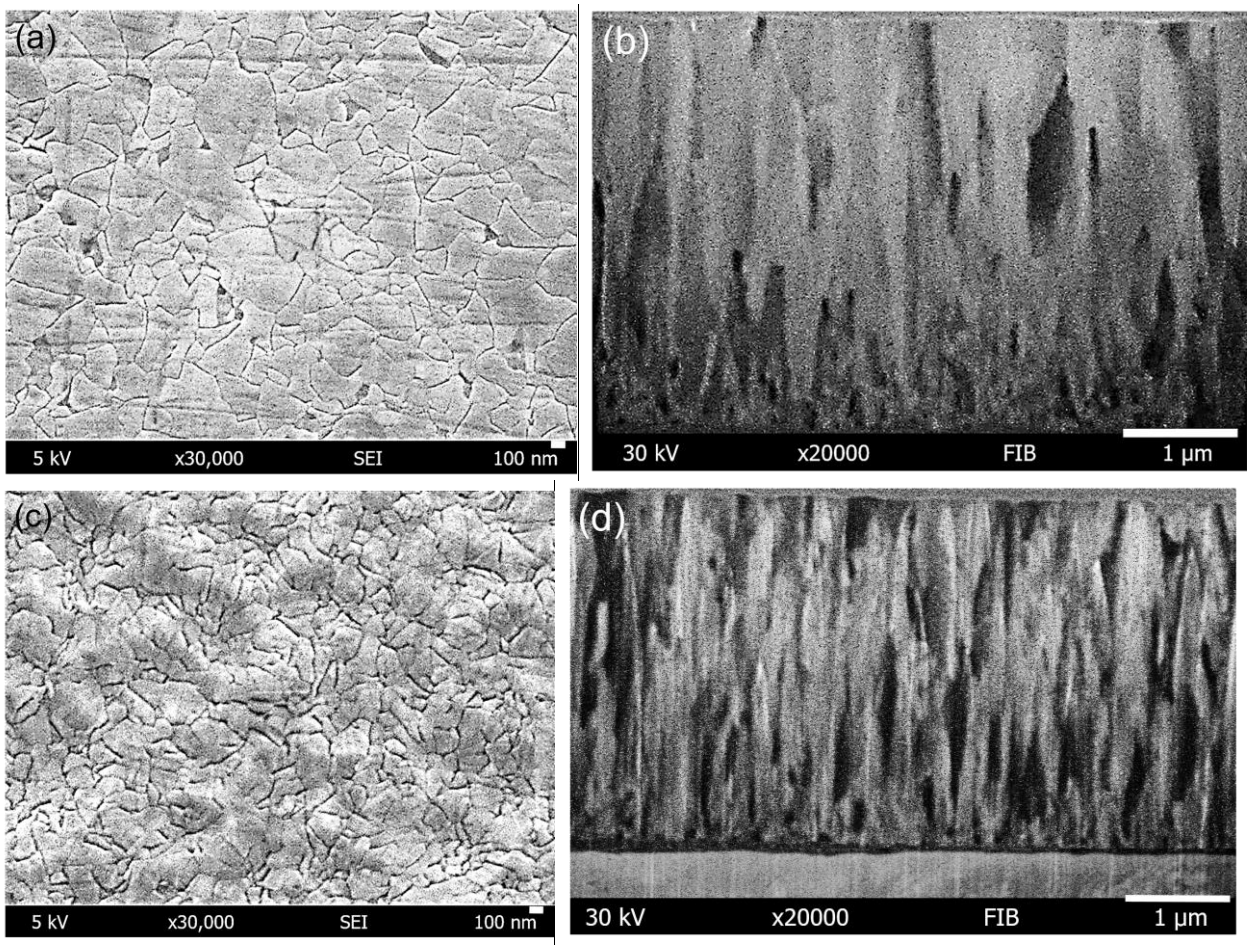

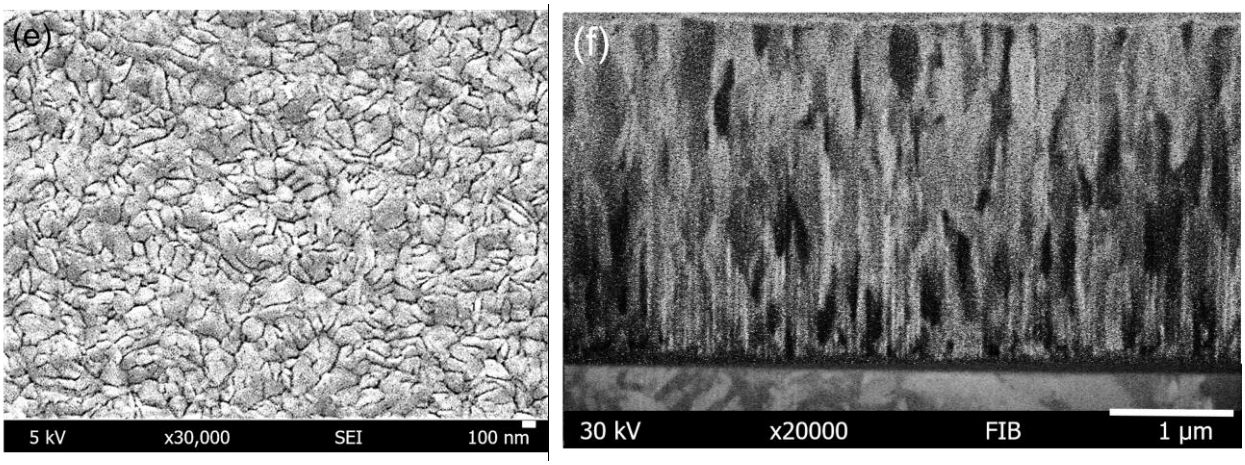

Figure 3. FESEM and FIB micrographs of etched coated surfaces and cross-sections of (a, b) DC-NA, (c, d) P1000-NA and (e, f) P1500-NA.

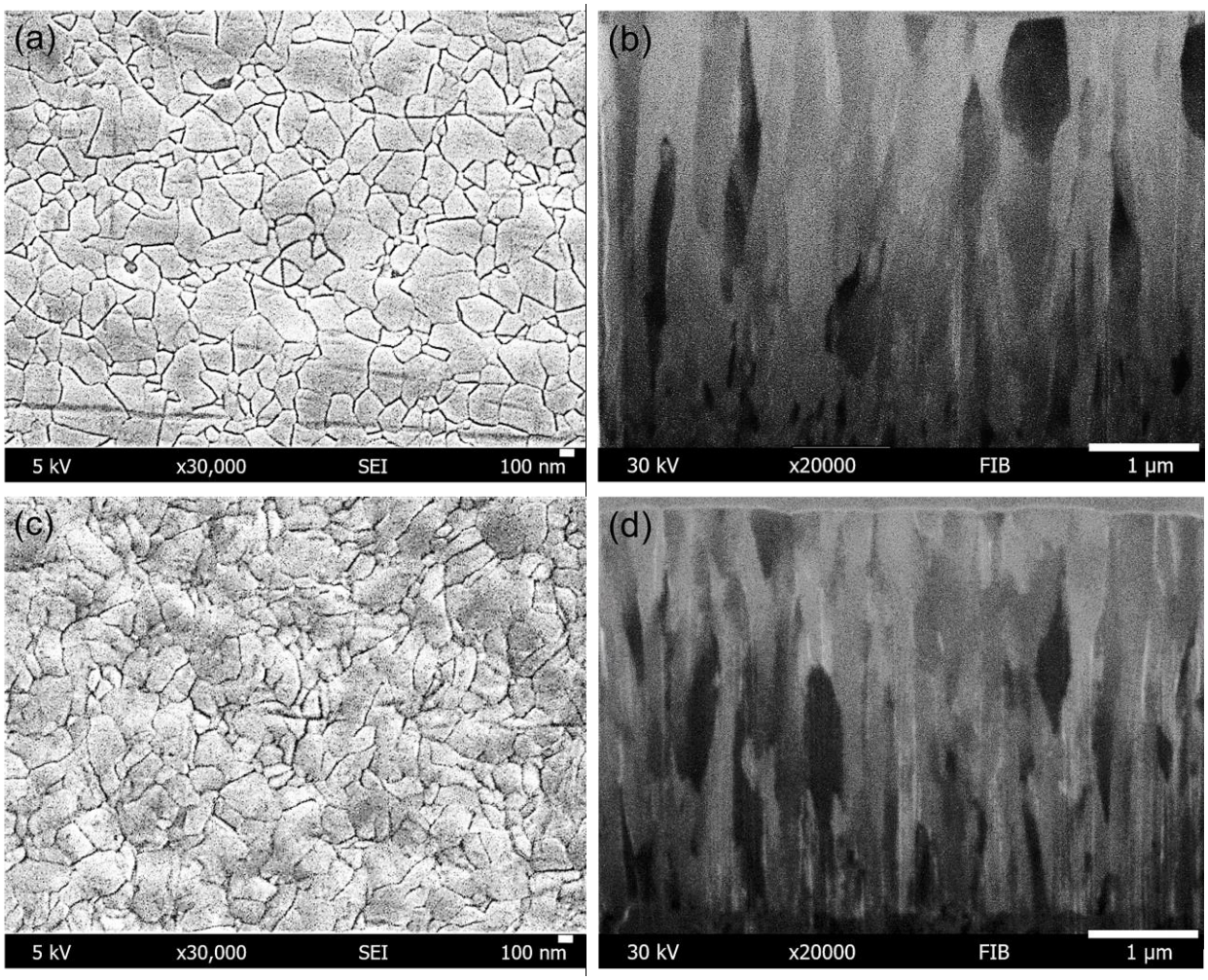

Figure 4. FESEM and FIB micrographs of etched coated surfaces cross-sections of (a, b) DC-N and (c, d) P1500-N.

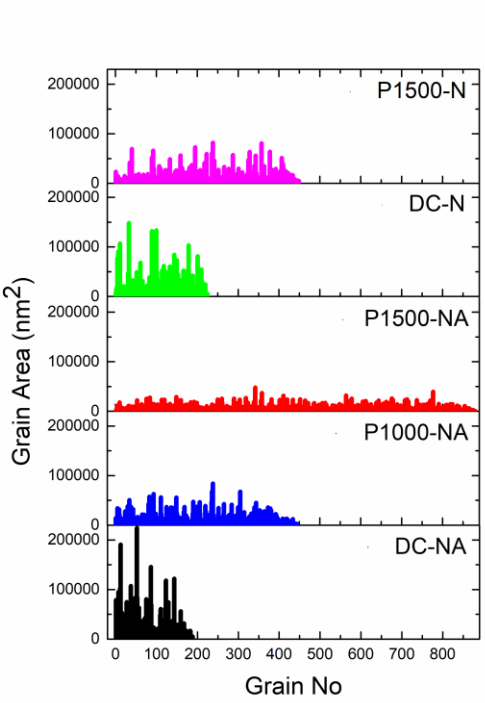

Figure 5. Distribution of grains area for samples coated in N_2+Ar atmosphere obtained by ImageJ program.

(220) preferred orientation was still preserved for coatings produced in pure nitrogen under -1500 V pulse bias (Fig. 2a). However, in this case, grain sizes were larger (Fig. 5). This result indicated the significant role of Ar on the observed structural changes. During the deposition process, the substrate surface is bombarded by both metal ions (Ti) emitted from the cathode, and gas ions (nitrogen and argon) generated by the collision of neutral gas atoms with the metal ion plasma. Acceleration of all types of ions occurs with the application of negative bias potential to the substrate [7, 31]. In the absence of Ar, the main contribution to the bombardment is from Ti ions since nitrogen ions are very light to render any substantial effect. Accordingly, under pulse bias application, the presence of Ar in the deposition environment during growth shows its effect by both increasing the nucleation sites at the initial stages of the coating, and increasing the adatom mobility during further growth of the film.

3.2. Stress Measurements

Residual stresses of the films that are determined from $\sin^2\psi$ method using glancing incidence XRD data (Fig. 1b and 2b) are presented in Table II. Additionally, XRD data and residual stress of the samples, which were heat treated in a vacuum at 700 ^{o}C to determine their responses to annealing, are presented in Fig. 1, 2 and Table II, respectively.

For the evaluation of bias potential-dependent stress build-up in TiN coatings, stress-generating components in thin films and their possible contributions will be summarised first. Total stress in a film is generated through intrinsic stresses (σ_i) and thermal stresses (σ_{th}) (Eq. 1) [13, 17, 32-34]. Intrinsic stress (σ_i) comprises three different stress components. The first one is growth stress (σ_{gs}) that is tensile and builds-up as a result of a reduction in the film volume. The magnitude of which decreases as the film thickness increases [17, 32, 33]. The second component is grain boundary contribution (σ_{gb}). This is related to the grain boundary interactions that are compressive for dense films, and its contribution increases with a decrease in the grain size (increase in the grain boundary length) [15-17, 32]. The third component is intra-grain contribution (σ_{intra}), originating from the introduction of volume defects as a result of the energetic bombardment of the film (atomic peening) and resulting in a lattice expansion (compressive stress) [16-18, 32].

$$\sigma_{tot} = \sigma_i + \sigma_{th} = (\sigma_{gs} + \sigma_{gb} + \sigma_{intra}) + \sigma_{th} \quad (1)$$

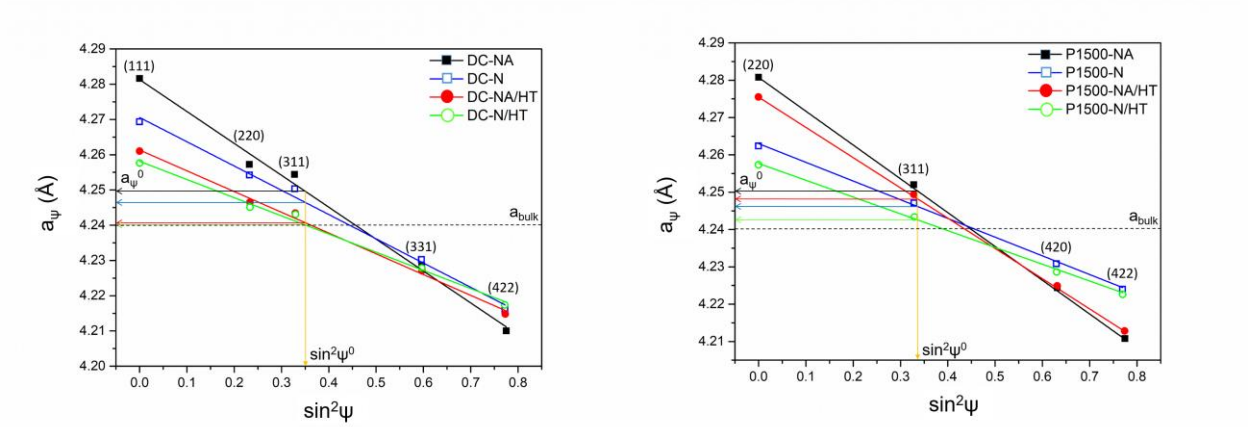

Figure 6. Lattice parameter vs $\sin^2\psi$ plots of TiN coated samples before and after annealing (a) DC-NA & DC-N samples and (b) P1500-NA & P1500-N samples: experimental data (symbols) and best-fit lines (full lines). Vertical line corresponds to stress-free direction $\sin^2\psi^0$ and horizontal lines correspond to stress-free lattice parameters (a_ψ^0).

All the samples used in this study experienced approximately the same thermal history during deposition and annealing, and the thickness of all of them was comparable. Therefore, the contribution of σ_{th} is expected to be similar and compressive for all the coatings. For thick films beyond few microns, the contribution of growth stresses starts to become lower [32-34]. Consequently, as the thickness of the films used in this study was in the range of 4-5 microns (thick films), the contribution of σ_{gs}, to the total stress is expected to be comparably lower [35]. Accordingly, stresses generated under different deposition conditions can be evaluated, mainly by taking into consideration the compressive stress-generating intrinsic components (σ_{gb} and σ_{intra}).

The comparison of stresses for coatings produced with DC bias in pure nitrogen (DC-N) and nitrogen + argon mixture (DC-NA), clearly showed that the presence of Ar in the deposition environment resulted in a 1.6 GPa increase in the compressive stress (Table II). As both of these coatings possess similar microstructure, the higher stress of DC-NA is mainly attributed to an increase in σ_{intra} because of the Ar ion bombardment-induced defects in the grains.

It is well known that annealing of TiN coatings at temperatures below $T/T_m = 0.5$ leads to recombination and annihilation of defects (point defects, dislocations, growth, and coalescence of subgrains). Accordingly, in the XRD patterns, shifting of the peaks towards unstrained values, reduction of peak broadening and more symmetric line profiles were observed [4, 35] (Fig. 1 and 2). Therefore, the annealing heat treatment conducted at 700 ^{o}C mainly resulted in the annihilation of the ion bombardment-induced intra-grain defects [36].

After the annealing heat treatment, the total stresses of the samples coated with DC bias (DC-NA & DC-N) became very close to each other (Fig. 6a and Table II). Furthermore, their stress-free lattice parameters (a_{ψ}^{0}) also became almost identical to a_{bulk}, as can be seen in a-$\sin^2\psi$ plots given in Fig. 6a. In fact, a_{ψ}^{0} lattice parameter extracted at the strain-free direction ($\sin^2\psi^{0}$) is a "stress-free but defect containing" lattice parameter related to the existence of the intra-grain stress component associated with the introduction of intra-grain defects [17]. These results indicated that the contribution of σ_{intra} to the residual stress was almost eliminated by this treatment.

For coatings deposited in N_2+Ar gas mixture, total stress increased by the application of -1000 V pulse bias and then decreased with the increase of pulse bias to -1500 V (Table II). The changes in the residual stress of the coatings, by applying different magnitudes of pulse bias voltage, are explained as a result of two simultaneous but differently directed processes: (1) stress generation due to ion implantation and defect production; (2) stress relaxation due to thermally activated processes of defect migration in the nonlocal thermoelastic peaks (NTP) of ions [7, 13]. According to this model, the stress reduction by the increase of pulse bias to -1500 V can be explained by the domination of stress relaxation effects. Although this model satisfies the observed changes in the stress level to some extent, it does not take into account the microstructural changes induced by applying different magnitudes of pulse bias voltage. The

contribution of grain boundary stress component (σ_{gb}) is expected to be significant because application of pulse bias results in the substantial changes in grain size (Fig. 3 &5). This contribution will be discussed further, by considering the stress measurement results of the coatings produced in pure N_2 and the annealed samples.

Comparision of the stress measurement results of TiN coating, produced with pulse bias with and without Ar in the deposition environment, also revelaed that presence of Ar resulted in an increase in the stress (Table II). However, stress increase induced by the presence of Ar was higher for samples produced with pulse bias when compared to the ones coated with DC bias. For coatings produced with -1500 V pulse bias, the difference in stress generated by the presence of Ar was 2.8 GPa (Table II). This is almost 2 times higher than the samples produced with DC bias, both with and without Ar in the deposition environment (Table II). This difference can be explained by the joint effects of the intra-grain defects (σ_{intra}) and decrease of grain sizes in the presence of Ar (σ_{gb}). For the coating produced using -1500 V pulse bias in the Ar-containing atmosphere (P1500-NA), grain sizes were distinctly smaller compared to P1500-N sample (Fig. 3e, f & 4c, d & 5). Therefore, an increase in the grain boundary length, created by the presence of Ar in the deposition environment, is expected to exert a higher contribution of grain boundary stress contrary to the ones produced with DC bias (Fig. 6a, b). Thus, higher compressive stress generation for the dense coatings which were produced with HVPB in the presence of Ar, can be explained by the increase of σ_{gb} contribution because of their longer grain boundary length.

More interesting results were obtained upon annealing of the coatings deposited by using HVPB. As explained before, this treatment is mainly expected to exert its effects on the relieving of intra-grain stress (σ_{intra}). Although a stress relief was also observed in the coatings produced with pulse bias, the magnitude of stress relief was lower than the coatings produced with DC bias (Table II). Especially for coatings produced with -1500 V pulse bias, the stress relief magnitudes

were significantly low (0.7 GPa for P1500-NA and 0.4 GPa for P1500-N). Additionally, the stress-free lattice parameter (a_ψ^0) of these coatings did not approach to a_{bulk} after annealing, contrary to the coatings produced with DC bias (Fig. 6a, b), indicating that intra-grain stress (σ_{intra}) was not totally released during annealing. This result can be explained by difficulty in annihilation of the intra-grain defects, because of the structural changes induced by HVPB. Some of the intra-grain defects, such as dislocations and subgrains, can be annihilated within the grains during the annealing by rearrangement, growth and coalescence. However, the annihilation of the point defects requires their movement to the grain boundaries. Migration of the point defects to the dense grain boundaries, created by the higher adatom mobility induced by the HVPB may require higher activation energy due to a decrease in the chemical potential differences between the grains and the grain boundaries. Thus, in this case, the low stress relief observed for these samples can be mainly attributed to the annihilation of intra-grain defects, with the exception of point defects which remained almost unchanged. Further studies are needed to clarify the observed differences in the stress-relieving behavior.

4. Conclusions

The results of this study revealed the significant influence of using HVPB on the preferred orientation, morphology and residual stress of TiN coatings produced with CA-PVD.

A change in the preferred orientation from (111) to (220) was observed along with a grain refinement and a relatively homogeneously-grown fine columnar structure. Presence of Ar in the deposition environment intensified the effects of HVPB.

The coatings produced with DC bias exhibited the expected Zone T structure, while the growth morphologies of the coatings produced using HVPB were very similar to the structures at the beginning of Zone II. This observation indicated that, by the application of short cycles of

high voltage pulses during the deposition process, the energy required for the restructuring was given to the system by increasing the adatom mobility.

When the presence of Ar in the deposition environment and its effects on the coatings produced with DC and pulse bias were compared, results indicated a higher stress generation in coatings produced with pulse bias. This observation, of the effects of Ar in coatings produced with pulse bias, can be explained by an increase of the grain boundary stress component (σ_{gb}), which is caused by significant grain size reduction.

For the coatings produced with DC bias, intra-grain stresses were almost totally annihilated, as is indicated by the approach of their strain-free lattice parameter to a_{bulk}. However, for the coatings produced with HVPB, especially for the ones deposited under -1500 V pulse bias, stress relief magnitudes were very low (0.4–0.7 GPa). Moreover, their stress free lattice parameters did not approach to a_{bulk} indicating that the conducted annealing treatment was not sufficient to relieve the intra-grain defects. The densification of the grain boundaries resulting in the decrease of chemical potential between the grains and grain boundaries was presented as the reason for the difficulty of migration of point defects to the grain boundaries.

Acknowledgements

This work has been supported within the scope of the bilateral project between The National Academy of Science of Ukraine (NASU) and the Scientific and Technological Research Council of Turkey (TUBITAK) (Contract No. 114M554). Valuable contributions of Dr. Vladimir Strel'nitskij and Dr. Elena Reshetnyak to stress measurements are sincerely acknowledged.

Disclosure Statement

No potential conflict of interest was reported by the authors.

References

[1] G. Abadias, Stress and preferred orientation in nitride-based PVD coatings, Surf. Coat. Technol. 202 (2008) 2223-2235.

[2] L.C. Hernández, L. Ponce, A. Fundora, E. López, E. Pérez, Nanohardness and Residual Stress in TiN Coatings, Materials, 4 (2011) 929-940.

[3] M. Tkadletz, N. Schalk, R. Daniel, J. Keckes, C. Czettl, C. Mitterer, Advanced characterization methods for wear resistant hard coatings: A review on recent progress, Surf. Coat. Technol. 285 (2016) 31-46.

[4] P.H. Mayrhofer, C. Mitterer, L. Hultman, H. Clemens, Microstructural design of hard coatings, Prog. Mater. Sci. 51 (2006) 1032-1114.

[5] S. Mukherjee, F. Prokert, E. Richter, W. Moller, Comparison of TiN and $Ti_{1-x}Al_xN$ coatings deposited on Al using plasma immersion ion implantation assisted deposition, Surf. Coat. Technol. 200 (2005) 2459-2464.

[6] S.S. Akkaya, V.V. Vasyliev, E.N. Reshetnyak, K. Kazmanlı, N. Solak, V.E. Strel'nitskij, M. Ürgen, Structure and properties of TiN coatings produced with PIII&D technique using high efficiency rectilinear filter cathodic arc plasma, Surf. Coat. Technol. 236 (2013) 332-340.

[7] V.V. Vasyliev, A.I. Kalinichenko, E.N. Reshetnyak, G.T.P. Azar, M. Ürgen, V.E. Strel'nitskij, Experimental and modeling study on the role of Ar addition to the working gas on the development of intrinsic stress in TiN coatings produced by filtered vacuum-arc plasma, Thin Solid Films, 642 (2017) 207-213.

[8] S. Akkaya, B. Yıldız, M. Ürgen, Orientation dependent tribological behavior of TiN coatings, J. Phys.: Condens. Matter. 28 (2016) 134009-134016.

[9] I. Petrov, P.B. Barna, L. Hultman, J.E. Greene, Microstructural evolution during film growth, J. Vac. Sci. Technol. A, 21 (2003) S117-S128.

[10] S. Mahieu, P. Ghekiere, D. Depla, R. De Gryse, Biaxial alignment in sputter deposited thin films, Thin Solid Films, 515 (2006) 1229-1249.

[11] R. Machunze, A.P. Ehiasarian, F.D. Tichelaar, G.C.A.M. Janssen, Stress and texture in HIPIMS TiN thin films, Thin Solid Films, 518 (2009) 1561-1565.

[12] V. Chawlaa, R. Jayaganthana, R. Chandra, Structural characterizations of magnetron sputtered nanocrystalline TiN thin films, Mater. Charact. 59 (2008) 1015-1020.

[13] S. Mukherjee, F. Prokert, E. Richter, W. Moller, Intrinsic stress and preferred orientation in TiN coatings deposited on Al using plasma immersion ion implantation assisted deposition, Thin

Solid Films, 445 (2003) 48-53.

[14] P.R. Guduru, E. Chason, L.B. Freund, Mechanics of compressive stress evolution during thin film growth, J. Mech. Phys. Solids. 51 (2003) 2127-2148.

[15] E. Chason, A kinetic analysis of residual stress evolution in polycrystalline thin films, Thin Solid Films 526 (2012) 1-14.

[16] E. Chason, P.R. Guduru, Tutorial: Understanding residual stress in polycrystalline thin films through real-time measurements and physical models, J. Appl. Phys. 119 (2016) 191101-1-21.

[17] L.E. Koutsokeras, G. Abadias, Intrinsic stress in ZrN thin films: Evaluation of grain boundary contribution from in situ wafer curvature and ex situ x-ray diffraction techniques, J. Appl. Phys. 111 (2012) 1-8.

[18] D. Magnfält G. Abadias, K. Sarakinos, Atom insertion into grain boundaries and stress generation in physically vapor deposited films, Appl. Phys. Lett. 103 (2013) 051910-1-4.

[19] U. Welzel, J. Ligot, P. Lamparter, A.C. Vermeulen, E.J. Mittemeijer, Stress analysis of polycrystalline thin films and surface regions by X-ray diffraction, J. Appl. Crystallogr. 38 (2005) 1-29.

[20] I.C. Noyan, J.B. Cohen, Residual stress, Springer-Verlag Inc., New York,1987.

[21] A. J. Perry, The state of residual stress in TiN films made by physical vapor deposition methods; the state of the art, J. Vac. Sci. Technol. A 8 (1990) 1351-1358.

[22] C.A. Schneider, W.S. Rasband, K.W. Eliceiri, NIH Image to ImageJ: 25 years of image analysis, Nature Methods, 9 (2012) 671-675.

[23] K. Khojier, H. Savaloni, E. Shokrai, Z. Dehghani, N. Zare Dehnavi, Influence of argon gas flow on mechanical and electrical properties of sputtered titanium nitride thin films, J. Theor. Appl. Phys. 7 (2013), 37-43.

[24] André Anders, A structure zone diagram including plasma-based deposition and ion etching, Thin Solid Films, Volume 518, Issue 15, 31 May 2010, Pages 4087-4090.

[25] U.C. Oh, J.H. Je, Effects of strain energy on the preferred orientation of TiN thin films, J. Appl. Phys. 74 (1993) 1692-1696.

[26] J. Pelleg, L.Z. Zervin, S. Lungo, N. Croitoru, Reactive-sputter-deposited TiN films on glass substrates, Thin Solid Films 197 (1991) 117-128.

[27] J.P. Zhao, X. Wang, Z.Y. Chen, S.Q. Yang, T.S. Shi and X.H. Liu, Overall energy model for preferred growth of TiN films during filtered arc deposition, J. Phys. D: Appl. Phys. 30 (1997) 5–12.

[28] Z. Yujuan, Y. Pengxun, W. Zhiguo, Z. Pingyu, Influences of deposition parameters on the microstructure and properties of nanostructural TiN films synthesized by filtered cathodic arc plasma, RARE METALS, 24 (2005) 370-375.

[29] P.B. Barna, M. Adamik, Fundamental structure forming phenomena of polycrystalline films and the structure zone models, Thin Solid Films, 317 (1998) 27–33.

[30] P. Patsalas, C. Gravalidis, S. Logothetidis, Surface kinetics and subplantation phenomena affecting the texture, morphology, stress, and growth evolution of titanium nitride films, J. Appl. Phys. 96 (2004) 6234-6246.

[31] A. Anders, Cathodic Arcs: From Fractal Spots to Energetic Condensation, Springer New York, 2010.

[32] R. Daniel, K.J. Martinschitz, J. Keckes, C. Mitterer, The origin of stresses in magnetron-sputtered thin films with zone T structures, Acta Mater. 58 (2010) 2621–2633.

[33] R. Daniel, J. Keckes, I. Matko, M. Burghammer, C. Mitterer, Origins of microstructure and stress gradients in nanocrystalline thin films: The role of growth parameters and self-organization, Acta Mater. 61 (2013) 6255–6266.

[34] J.-D. Kamminga, Th. H. de Keijser, R. Delhez, E. J. Mittemeijer, On the origin of stress in magnetron sputtered TiN layers, J. Appl. Phys. 88 (2000) 6332-6345.

[35] D. Magnfält, A. Fillon, R.D. Boyd, U. Helmersson, K. Sarakinos, G. Abadias, Compressive intrinsic stress originates in the grain boundaries of dense refractory polycrystalline thin films, J. Appl. Phys. 119 (2016) 055305-1-7.

[36] M. Urgen, A.F. Cakir, The effect of heating on corrosion behavior of TiN- and CrN-coated Steels, Surf. Coat. Technol. 96 (1997) 236-244.

[37] I. Petrov, L. Hultman, J.-E. Sundgren, and J.E. Greene, Polycrystalline TiN films deposited by reactive bias magnetron sputtering: Effects of ion bombardment on resputtering rates, film composition, and microstructure, J. Vac. Sci. Technol. A, 10 (1992) 265-272.

Table I. Deposition parameters, samples coding, coatings thicknesses and calculated average grain areas of the TiN coatings produced with DC and pulse bias.

	Bias Voltage Type-Magnitude (V)	Pulse Bias Duty Cycle (%)	Coating Atmosphere	Coatings Thickness (μm)	Average Grain Area (nm^2)
DC-NA	DC-150	-	N_2+20%Ar	4.9±0.1	22,032
P1000-NA	Pulse-1000	14	N_2+20%Ar	4.1±0.1	11,092
P1500-NA	Pulse-1500	14	N_2+20%Ar	3.7±0.2	6,057
DC-N	DC-150	-	N_2	5.2±0.2	20,278
P1500-N	Pulse-1500	14	N_2	4.4±0.2	11,079

Table II. Residual stress of as-deposited and heat-treated TiN coated samples.

	As-deposited Stress (GPa)	As-deposited Hardness (GPa)	Stress after Heat Treatment (GPa)	Stress Release (GPa)
DC-NA	-7±0.5	36.5±0.6	-4.5±0.4	2.5
P1000-NA	-8.2±0.4	31.5±0.7	-6.5±0.4	1.5
P1500-NA	-7.5±0.4	29.5±0.2	-6.8±0.4	0.7
DC-N	-5.4±0.3	32.8±0.7	-4±0.2	1.4
P1500-N	-4.2±0.2	27.5±0.2	-3.8±0.2	0.4

Figure Captions

Figure 1. XRD patterns of TiN coatings deposited using different bias voltages in N_2+Ar atmosphere before and after heat treatment in (a) θ-2θ and (b) GI modes.

Figure 2. XRD patterns of TiN coatings deposited using different bias voltages in pure N_2 gas before and after heat treatment in (a) θ-2θ and (b) GI modes.

Figure 3. FESEM and FIB micrographs of etched coated surfaces and cross-sections of (a, b) DC-NA, (c, d) P1000-NA and (e, f) P1500-NA.

Figure 4. FESEM and FIB micrographs of etched coated surfaces cross-sections of (a, b) DC-N and (c, d) P1500-N.

Figure 5. Distribution of grains area for samples coated in N_2+Ar atmosphere obtained by ImageJ program.

Figure 6. Lattice parameter vs $\sin^2\psi$ plots of TiN coated samples before and after annealing (a) DC-NA & DC-N samples and (b) P1500-NA & P1500-N samples: experimental data (symbols) and best-fit lines (full lines). Vertical line corresponds to stress-free direction $\sin^2\psi^0$ and horizontal lines correspond to stress-free lattice parameters (a_ψ^0).